

FlexControl: Computation-Aware ControlNet with Differentiable Router for Text-to-Image Generation

Zheng Fang¹ Lichuan Xiang^{1,2} Xu Cai² Kaicheng Zhou² Hongkai Wen¹

¹University of Warwick ²ColloV Labs

zheng.fang.6, lichuan.xiang.3, hongkai.wen@warwick.ac.uk,
caitree@gmail.com, caseyz@collov.com

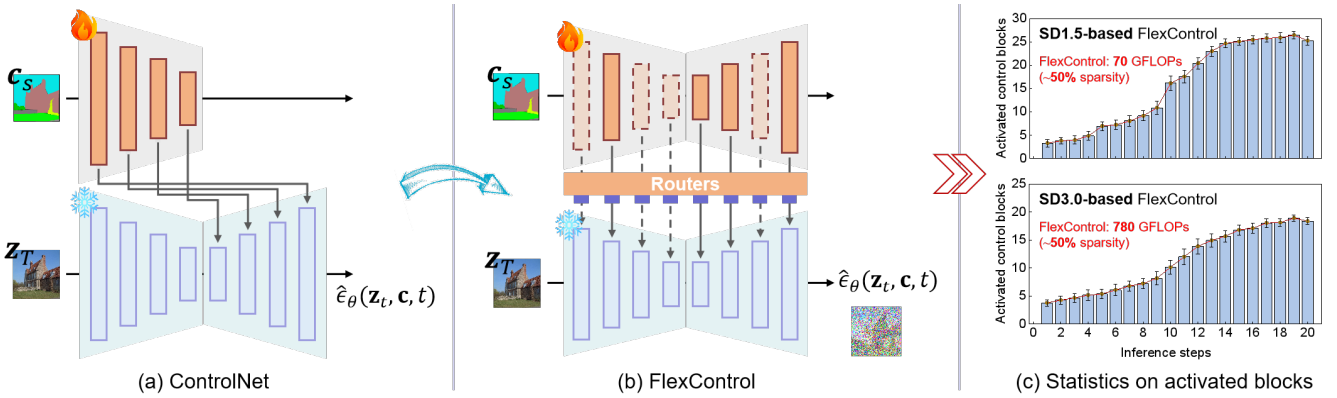


Figure 1. **Dynamically control image generation based on timestep and specific sample.** (a) The architecture of ControlNet. (b) The architecture of proposed FlexControl. (c) Statistics on the number of activated control blocks of FlexControl at each denoising step. Here, “50% sparsity” indicates that the number of floating-point operations (FLOPs) of activated blocks is limited to 50% of the trainable branch.

Abstract

ControlNet offers a powerful way to guide diffusion-based generative models, yet most implementations rely on ad-hoc heuristics to choose which network blocks to control—an approach that varies unpredictably with different tasks. To address this gap, we propose FlexControl, a novel framework that copies all diffusion blocks during training and employs a trainable gating mechanism to dynamically select which blocks to activate at each denoising step. With introducing a computation-aware loss, we can encourage control blocks only to activate when it benefit the generation quality. By eliminating manual block selection, FlexControl enhances adaptability across diverse tasks and streamlines the design pipeline, with computation-aware training loss in an end-to-end training manner. Through comprehensive experiments on both UNet (e.g., SD1.5) and DiT (e.g., SD3.0), we show that our method outperforms existing ControlNet variants in certain key aspects of interest. As evidenced by both quantitative and qualitative evaluations, FlexControl preserves or enhances image fidelity while also reducing computational overhead by selectively activating the most relevant blocks. These results underscore the potential of a

flexible, data-driven approach for controlled diffusion and open new avenues for efficient generative model design.

1. Introduction

Diffusion-based image generation models have recently gained widespread acceptance in the art and design community, not only for their high-quality, photo-realistic image generation but also due to the transformative capabilities of from controllable unit like ControlNet [56], T2I-Adapter [32], etc, which enables users to create images under diverse conditions (e.g., layout, pose, shape, and form), allows generated image that satisfied various real-world demand.

Despite its growing popularity, ControlNet methods typically rely on multiple design hyperparameters—such as choosing which network block to control for improved fidelity and adherence to input conditions—without a systematic investigation of their effects. For example, the ControlNet variant based on SD1.5 [50] replicates encoder blocks and injects control information into the decoder, whereas T2I-Adapter applies control in the encoder. It remains unclear which block-level configuration is most ef-

fective, especially since optimal designs can vary by task. Complicating matters further, ControlNet is often trained on significantly smaller datasets than those used for the diffusion model’s pre-training, implying that adding too much control could disrupt the pretrained representations and degrade image quality, since insufficient control may fail to deliver the desired guidance. As an evidence, a recent study [22] highlights that the number and placement of control blocks might significantly affect image quality in tasks such as inpainting. Moreover, in practice, ControlNet pipeline relies on heuristic strategies to decide which timesteps should receive control signals at inference, yet evidence is scarce regarding which approach consistently yields the best results. Collectively, these gaps emphasize the need for a more principled, comprehensive analysis of ControlNet design and inference strategies.

To dynamically adjust control blocks based on timestep and conditional information while maintaining (or even improving) generation quality, we propose FlexControl, a data-driven dynamic control method. Similar to conventional controllable generation methods, as shown in Fig. 1(a), we freeze the original diffusion model and copy its parameters to process task-specific conditional images. FlexControl is equipped with a router unit within the control block (see Fig. 1(b)) to plan forward routes, activating control blocks only when necessary based on the current latent variable. In contrast to other controllable generation models, FlexControl customizes the inference path for each input, minimizing potential redundant computations. In summary, our main contributions are as follows:

1. Data-driven dynamic control configuration: We introduce an automated router unit that dynamically selects control blocks at each timestep, eliminating the need for exhaustive architecture searches and retraining. Our approach enables: (1) task-adaptive control configurations through end-to-end training, (2) temporally adaptive inference via per-timestep activation decisions, and (3) faster configuration design compared to manual search baselines by removing the need for configuration search and repeated training.

2. Computation-aware controllable generation: Our approach significantly enhances controllability and image quality while maintaining a similar computational cost to the original ControlNet by introducing a novel computation-aware training loss. Specifically, in the depth-map control task, our method achieves a 6.11 FID improvement and a 6.30% RMSE reduction. Furthermore, this strategic allocation of computation to control units outperforms brute-force doubling, establishing new Pareto frontiers in the control-quality v.s. compute trade-off.

3. Universal plug-and-play integration: Our method seamlessly integrates with any dual-stream control-architecture, introducing minimal additional parameters and zero architectural modifications to host models. It enables flexible switching between full control and efficiency-optimized modes, depending on computational requirements.

2. Related Work

Text-to-image diffusion models. The diffusion probabilistic model was originally introduced by Sohl-Dickstein *et al.* [48], which has been successfully applied in the field of image synthesis and achieved impressive results [7, 18–20, 24, 43]. The Latent Diffusion Models (LDMs) [44], reduce computational demands by transferring the diffusion process from the pixel space to the latent feature space. Such diffusion models [33, 36, 44, 46, 50] typically encode text prompts as potential vectors through pre-trained language models [38, 39], combined with UNet [45] to predict noise to remove at each timestep. Recent studies explore Transformer-based architectures, which have yielded state-of-the-art results for large-scale text-to-image generation tasks [1, 2, 11, 34, 51]. These frameworks leverage Transformers’ capacity for modeling long-range dependencies and scaling to massive multimodal datasets, enabling breakthroughs in compositional reasoning, dynamic resolution adaptation, and high-fidelity synthesis. However, their reliance on purely textual input—despite advances in cross-modal alignment—still poses challenges for precise spatial or stylistic control.

Controllable diffusion models. While state-of-the-art text-to-image models achieve remarkable photorealism, their reliance on inherently low-bandwidth, abstract textual input limits their ability to meet the nuanced and complex demands of real-world artistic and design applications. This underscores the growing need for frameworks like ControlNet [56] and T2I-Adapter [32], which augment text prompts with spatial or structural constraints (*e.g.*, sketches, depth maps, or poses), enabling finer-grained control over generation to bridge the gap between creative intent and algorithmic output. Recent advancements in controllable text-to-image generation have diversified across methodological approaches. Instance-based methods, such as those by [53, 60] enable zero-shot generation of stylized images from a single reference input, prioritizing speed and flexibility. Meanwhile, an improvement in cross-attention constraint, proposed by [4], guides generation along desired trajectories by refining latent space interactions. Prompt engineering has also emerged as a lightweight strategy for enhancing controllability, with works like [21, 27, 54, 57] optimizing textual or hybrid prompts for fine-grained guidance. Additionally, multi-condition frameworks [17, 26, 37, 58] inte-

grate auxiliary inputs—such as segmentation maps or depth cues—to complement text prompts, improving alignment with complex user intent. However, while these methods expand generative versatility, many overlook the computational overhead introduced by auxiliary networks, limiting their scalability for real-time applications.

Improving ControlNet efficiency. Efforts to enhance ControlNet’s efficacy and efficiency have focused on architectural redesigns, training optimizations, and inference acceleration. ControlNeXt [35] replaces ControlNet’s bulky auxiliary branches with a streamlined architecture and substitutes zero convolutions with Cross Normalization, slashing learnable parameters by 90% while maintaining stable convergence. Beyond architecture, multi-expert diffusion frameworks [25, 55] tailor denoising operations to specific timesteps, though their computational demands hinder practicality. To reduce inference costs, pruning techniques [12, 13, 23] trim redundant parameters from pre-trained denoising models, while distillation methods [16] train lightweight guide models to minimize denoising steps. Inspired by RepVGG [8], RepControlNet [6] introduces a novel reparameterization strategy: modal-specific adapters modulate features during training, and their weights are later merged with the base network, eliminating auxiliary computations at inference. Unlike prior methods that rely on fixed heuristics, post-hoc pruning, or static architectural modifications, our FlexControl introduces a dynamic, end-to-end trainable framework where block activation is both task-aware and computation-aware. By integrating a gating mechanism with a computational efficiency objective, our approach uniquely balances precision and resource usage, enabling adaptive control across diverse architectures (UNet, DiT) without manual intervention — a paradigm shift from rigid, task-specific designs to flexible, generalizable control.

3. Methodology

3.1. Preliminaries

Denoising diffusion probabilistic model (DDPM) [15] aims to approximate the real data distribution $q(\mathbf{x}_0)$ with the learned model distribution $p(\mathbf{x}_0)$ [15]. It contains a forward diffusion process that progressively adds noise to the image and a reverse generation process that synthesizes the image by progressively eliminating noise. Formally, the forward process is a T -step Markov chain:

$$q(\mathbf{x}_{1:T}|\mathbf{x}_0) := \prod_{t=1}^T q(\mathbf{x}_t|\mathbf{x}_{t-1}), \quad (1)$$

$$q(\mathbf{x}_t|\mathbf{x}_{t-1}) := \mathcal{N}(\mathbf{x}_t; \sqrt{1 - \beta_t}\mathbf{x}_{t-1}, \beta_t \mathbf{I}),$$

where $\{\beta_t\}_{t=0}^T$ are the noise schedule, and $\{\mathbf{x}_t\}_{t=0}^T$ are latent variables. Let $\alpha_t = 1 - \beta_t$, the distribution of \mathbf{x}_t for a given \mathbf{x}_0 can be expressed as:

$$q(\mathbf{x}_t|\mathbf{x}_0) := \mathcal{N}(\mathbf{x}_t; \sqrt{\bar{\alpha}_t}\mathbf{x}_0, (1 - \bar{\alpha}_t) \mathbf{I}). \quad (2)$$

Here, $\bar{\alpha}_t = \prod_{i=0}^t \alpha_i$ is a differentiable function of timestep t , which is determined by the denoising sampler. Therefore, the diffusion training loss can be formulated as:

$$\mathcal{L}_\theta = \mathbb{E}_{\mathbf{x}_0, t \sim \mathcal{U}(t), \epsilon \sim \mathcal{N}(\mathbf{0}, \mathbf{I})} \left[w(\lambda_t) \|\hat{\epsilon}_\theta(\mathbf{x}_t, t) - \epsilon\|_2^2 \right], \quad (3)$$

where ϵ denotes a noise vector drawn from a Gaussian distribution, and $\hat{\epsilon}_\theta$ refers to the predicted noise at timestep t by denoising model with parameters θ . $w(\lambda_t)$ is a pre-defined weighted function that takes into the signal-to-noise ratio λ_t . The reverse process first sample a Gaussian noise $p(\mathbf{x}_T) = \mathcal{N}(\mathbf{x}_T; \mathbf{0}, \mathbf{I})$, and then proceeding with the transition probability density step by step:

$$p_\theta(\mathbf{x}_{t-1}|\mathbf{x}_t) \approx q(\mathbf{x}_{t-1}|\mathbf{x}_t, \mathbf{x}_0) = \mathcal{N}(\mathbf{x}_{t-1}; \mu_\theta(\mathbf{x}_t, \mathbf{x}_0), \sigma_t^2 \mathbf{I}), \quad (4)$$

where $\mu_\theta(\mathbf{x}_t, \mathbf{x}_0) = \frac{1}{\sqrt{\alpha_t}} \left(\mathbf{x}_t - \frac{1 - \alpha_t}{\sqrt{1 - \alpha_t}} \epsilon_\theta(\mathbf{x}_t, t) \right)$ and $\sigma_t^2 = \frac{1 - \bar{\alpha}_{t-1}}{1 - \bar{\alpha}_t} \beta_t$ are the mean and variance of posterior Gaussian distribution $p_\theta(\mathbf{x}_0)$.

In order to improve the efficiency of diffusion model, flow-based optimization strategy [28, 30, 31] is introduced, which defines the forward process as a straight path between the real data distribution and the standard normal distribution:

$$\mathbf{x}_t = a_t \mathbf{x}_0 + b_t \epsilon. \quad (5)$$

With Eq. (5), a vector field u_t is constructed to generate a path p_t between the noise distribution and the data distribution. Meanwhile, the velocity v is parameterized by the weight θ of a neural network to approximate u_t . After variable recombination, the flow matching object can also be formulated as Eq. (3) [10]. In the reverse stage, flow matching uses ODE solver for fast sampling:

$$\mathbf{x}(t) = \mathbf{x}(0) + \int_0^t v_\theta(\mathbf{x}(\tau), \tau) d\tau. \quad (6)$$

3.2. Structure

Building on the core design philosophy of ControlNet, we first fix the powerful diffusion model backbone, fine-tune a trainable copy with zero module to learn conditional controls, and then inject the acquired knowledge into the frozen backbone:

$$\mathbf{y} = \mathcal{F}(\mathbf{x}; \Theta) + \mathcal{Z}(\mathcal{F}(\mathbf{x} + \mathcal{Z}(\mathbf{c}; \Theta_{z1}); \Theta_c); \Theta_{z2}), \quad (7)$$

where Θ and Θ_c are the weight parameters of the original block and the trainable copy respectively, \mathcal{Z} represents zero

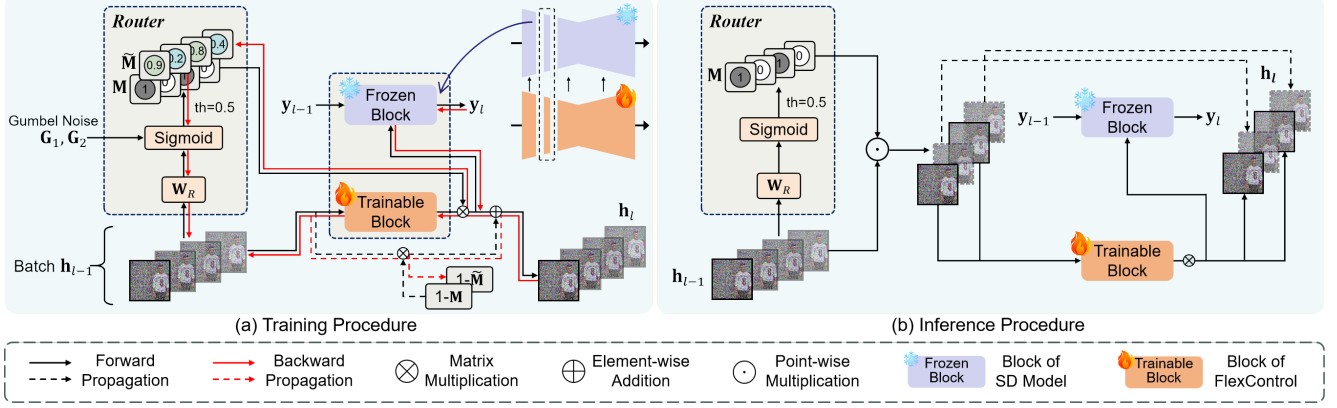


Figure 2. **Overview of dynamic routing guided by router unit.** (a) In the training stage, Gumbel noise is added to the discrete mask to assist the gradient backpropagation. (b) In the inference stage, the router unit controls whether to activate the control block according to the input latent variable. Once output the instruction of inactive, the corresponding control block and zero module will be skipped.

module and \mathbf{c} is the control element. Instead of just cloning the encoder and adding conditional controls only in the decoder blocks [56], as shown in Fig. 1(a), we copy all blocks of the original diffusion model to generate conditional controls and inject them into the corresponding blocks of the backbone in turn, as shown in Fig. 1(b), which is similar to the strategy used in BrushNet [22], and we call this structure ControlNet-Large. Although the double branch structure improves the quality of the generated image, it leads to huge redundant computation and multiplies the inference delay.

To reduce computational redundancy and enhance image generation quality, we propose FlexControl, which introduces a lightweight router unit before each conditional control generation block in the trainable branch. The router generates a binary mask $\mathcal{M} \in \{0, 1\}^N$ from the input latent feature, determining whether the underlining control block needs to be activated. Specifically, “0” indicates inactive, “1” indicates activate, and N represents the number of control blocks in the trainable branch.

The mask generation process of the router is data-driven, enabling independent path planning and adaptive decision-making based on the input latent representation. As shown in Fig. 2, during inference, if the router outputs a mask value of “0”, the conditional mapping skips the next control block until activation is deemed necessary. Taking the l -th control block as an example, the computation process can be formulated as:

$$\mathbf{h}_l = \begin{cases} \mathcal{F}_l(\mathbf{h}_{l-1}, \mathbf{c}, t; \Theta_c^l) & \text{if } \mathcal{M}_l = 1 \\ \text{skip}_l(\mathbf{h}_{l-1}) & \text{if } \mathcal{M}_l = 0, \end{cases} \quad (8)$$

where $\mathcal{F}_l(\cdot)$ indicates the l -th control block operation with parameter Θ_c^l , \mathbf{h}_l is the output of it at timestep t , and $\text{skip}_l(\cdot)$ is used to bypass the current block. Following the design of [56], we utilize the zero module to transform the

latent feature \mathbf{h}_l into conditional control:

$$\mathbf{y}_c^l = \begin{cases} \mathcal{Z}_l(\mathbf{h}_l; \Theta_z^l) & \text{if } \mathcal{M}_l = 1 \\ \text{N/A} & \text{if } \mathcal{M}_l = 0. \end{cases} \quad (9)$$

Here, \mathbf{y}_c^l denotes the conditional control incorporated into the feature space of the backbone.

Remark: The above designed router is in fact lightweight, accounting for less than 1% of the parameters of the overall model. Since the skipped parameters are excluded from tensor computation during inference, FlexControl barely introduces computational burden by adaptively adjusting the number of active control blocks. See the detailed inference process in Algorithm 1 in Sec. A1.

3.3. Router unit design

As illustrated earlier, the router unit is lightweight and plug-and-play to any diffusion architecture. However, given the differences between UNet and DiT, we will discuss the implementation of the router on these two commonly used architectures separately.

Router for UNet-based architecture. The output of UNet block is a multi-channel spatial feature. Given input $\mathbf{h} \in \mathbb{R}^{C \times H \times W}$, the router unit first transforms the spatial feature into linear feature $\mathbf{h}' \in \mathbb{R}^C$ through the downsampling layer, we use global average pooling (GAP) in implementation, and then the MLP layer with weight $\mathbf{W} \in \mathbb{R}^{C \times 1}$ maps the linear feature into a scalar \mathcal{K} :

$$\mathcal{K} = \text{MLP}(\text{GAP}(\mathbf{h})). \quad (10)$$

Henceforth, we compute a new scalar \mathcal{K}' by restricting the value of \mathcal{K} to the interval $(0, 1)$ through the Sigmoid function. In order to convert \mathcal{K}' into a binary coding, we introduce a threshold discriminator to control the generation of

the mask \mathcal{M} by a preset threshold \mathcal{T} (0.5 by default):

$$\mathcal{M} = \begin{cases} 1 & \text{if } \mathcal{K}' > \mathcal{T} \\ 0 & \text{if } \mathcal{K}' \leq \mathcal{T}. \end{cases} \quad (11)$$

We multiply the mask \mathcal{M} and the output latent feature to zero out the corresponding control block and zero module. It can be seen from the above description that the mask \mathcal{M} is learned from the latent variable \mathbf{h} . Since timestep embedding is introduced into the blocks of the diffusion model during the generation of \mathbf{h} , the output of the router is also affected by the sampled timesteps.

Router for DiT-based architecture. For the router applied in DiT, we conduct feature analysis from multiple perspectives. Specifically, we perform both global and local feature encoding on the latent variable $\mathbf{h} \in \mathbb{R}^{N \times C}$ output by the Transformer block [41, 42]. The detailed encoding process is as follows:

$$\mathbf{h}^{global} = \text{MLP}^{global}(\text{AVG}_{dim=1}(\mathbf{h})), \quad (12)$$

$$\mathbf{h}^{local} = \text{MLP}^{local}(\text{AVG}_{dim=2}(\mathbf{h})). \quad (13)$$

From Eqs. (12) and (13), the encoding process for global and local features primarily consists of two steps. First, feature fusion is performed across all tokens and hidden channels using the function $\text{AVG}(\cdot)$, which is implemented via average pooling along different dimensions of latent variable. This yields the global feature $\mathbf{z}^{global} \in \mathbb{R}^C$ and local feature $\mathbf{z}^{local} \in \mathbb{R}^N$. Second, the embedding dimensions of \mathbf{z}^{global} and \mathbf{z}^{local} are aligned through an MLP layer and reduced to \mathcal{O} , which is set to $C/64$ by default. Intuitively, the local feature captures token-specific information, while the global feature encodes potential relationships between tokens. We then merge these global and local features to form a new feature representation:

$$\mathbf{h}^{mix} = \alpha_1 \cdot \mathbf{h}^{global} + \alpha_2 \cdot \mathbf{h}^{local}. \quad (14)$$

In the above equation, α_1 and α_2 are weight factors that balance the influence of global and local features, both set to 0.5 by default. The fused feature variable $\mathbf{h}_{l-1}^{mix} \in \mathbb{R}^{\mathcal{O}}$ is then passed through an MLP layer to produce \mathcal{K} . At the end, \mathcal{K} is processed through a Sigmoid layer followed by the threshold discriminator described in Eq. (11), resulting in the router mask \mathcal{M} .

3.4. End-to-end training

Differentiable learning of router. To enable end-to-end training via gradient descent, we address the discrete, non-differentiable nature of the mask by incorporating Gumbel noise into the Sigmoid activation function. This allows the

discrete mask \mathcal{M} to be approximated by the differentiable Gumbel-Sigmoid version $\widetilde{\mathcal{M}}$ during training:

$$\widetilde{\mathcal{M}}_l = \text{Sigmoid}\left(\frac{\mathcal{R}_l(\mathbf{h}_{l-1}; \Theta_{\mathcal{R}}^l) + G_1 - G_2}{\mathcal{TP}}\right), \quad (15)$$

where $G_1, G_2 \sim \text{Gumbel}(0, 1)$, \mathcal{TP} denotes the temperature hyperparameter (5 by default), $\mathcal{R}(\cdot)$ denotes tensor computations in the router unit parameterized by $\Theta_{\mathcal{R}}$.

To this end, we employ different mask schemes during the forward and backward passes:

$$\mathbf{h}_l = \begin{cases} \mathcal{F}_l \cdot \mathcal{M}_l + \text{skip}_l(\mathbf{h}_{l-1}) \cdot (1 - \mathcal{M}_l) & \text{if Forward} \\ \mathcal{F}_l \cdot \widetilde{\mathcal{M}}_l + \text{skip}_l(\mathbf{h}_{l-1}) \cdot (1 - \widetilde{\mathcal{M}}_l) & \text{if Backward.} \end{cases} \quad (16)$$

Meanwhile, the computation process of the zero module is adjusted accordingly:

$$\mathbf{y}_c^l = \begin{cases} \mathcal{Z}_l(\mathbf{h}_l; \Theta_z^l) \cdot \mathcal{M}_l & \text{if Forward} \\ \mathcal{Z}_l(\mathbf{h}_l; \Theta_z^l) \cdot \widetilde{\mathcal{M}}_l & \text{if Backward.} \end{cases} \quad (17)$$

Remark: As can be seen in Eqs. (16) and (17) during training, the blockwise routing differs from the inference process displayed in Eqs. (8) and (9): during training, we retain all blocks to ensure proper back-propagation, rather than skipping blocks as done during inference.

Computation-aware training loss. Following standard controllable generation methods, our training dataset \mathcal{D} contains triples of the original image x , spatial conditioning control \mathbf{c}_s , and text prompt \mathbf{c}_t . The diffusion loss of FlexControl is formulated as:

$$\mathcal{L}_{\text{SD}} = \mathbb{E}_{\mathbf{x}_0, \mathbf{c}_t, \mathbf{c}_s, t, \epsilon \sim \mathcal{N}(0, I)} \left[\|\hat{\epsilon}_\theta(\mathbf{x}_t, \mathbf{c}_t, \mathbf{c}_s, t) - \epsilon\|_2^2 \right]. \quad (18)$$

FlexControl aims to activate the optimal control blocks and inject conditional mapping into the backbone network for efficient image generation. In addition to the regular diffusion loss \mathcal{L}_{SD} , we introduce a cost loss \mathcal{L}_C to regulate resource consumption to the desired sparsity γ , which measures the proportion of floating-point operations (FLOPs):

$$\mathcal{L}_C = \frac{1}{|\mathcal{D}_{\text{bs}}|} \sum_{d \in \mathcal{D}_{\text{bs}}} \left(\frac{F_{t_d}^{\text{Flex}}(d)}{F_{t_d}^{\text{Large}}(d)} - \gamma \right)^2, \quad (19)$$

where \mathcal{D}_{bs} represents the current batch samples, $t_d \in [0, T]$ is the uniformly sampled timestep for sample d . $F_t(d)$ denotes FLOPs of the trainable branch at sampled timestep, and superscripts Flex and Large respectively denote FlexControl and ControlNet-Large. We combine \mathcal{L}_{SD} and \mathcal{L}_C to bring out the final optimization goal,

$$\mathcal{L}_\theta = \mathcal{L}_{\text{SD}} + \lambda_C \cdot \mathcal{L}_C, \quad (20)$$

where λ_C is the hyperparameter that controls the influence of loss \mathcal{L}_C . See the detailed training process in Algorithm 2 in Sec. A1.

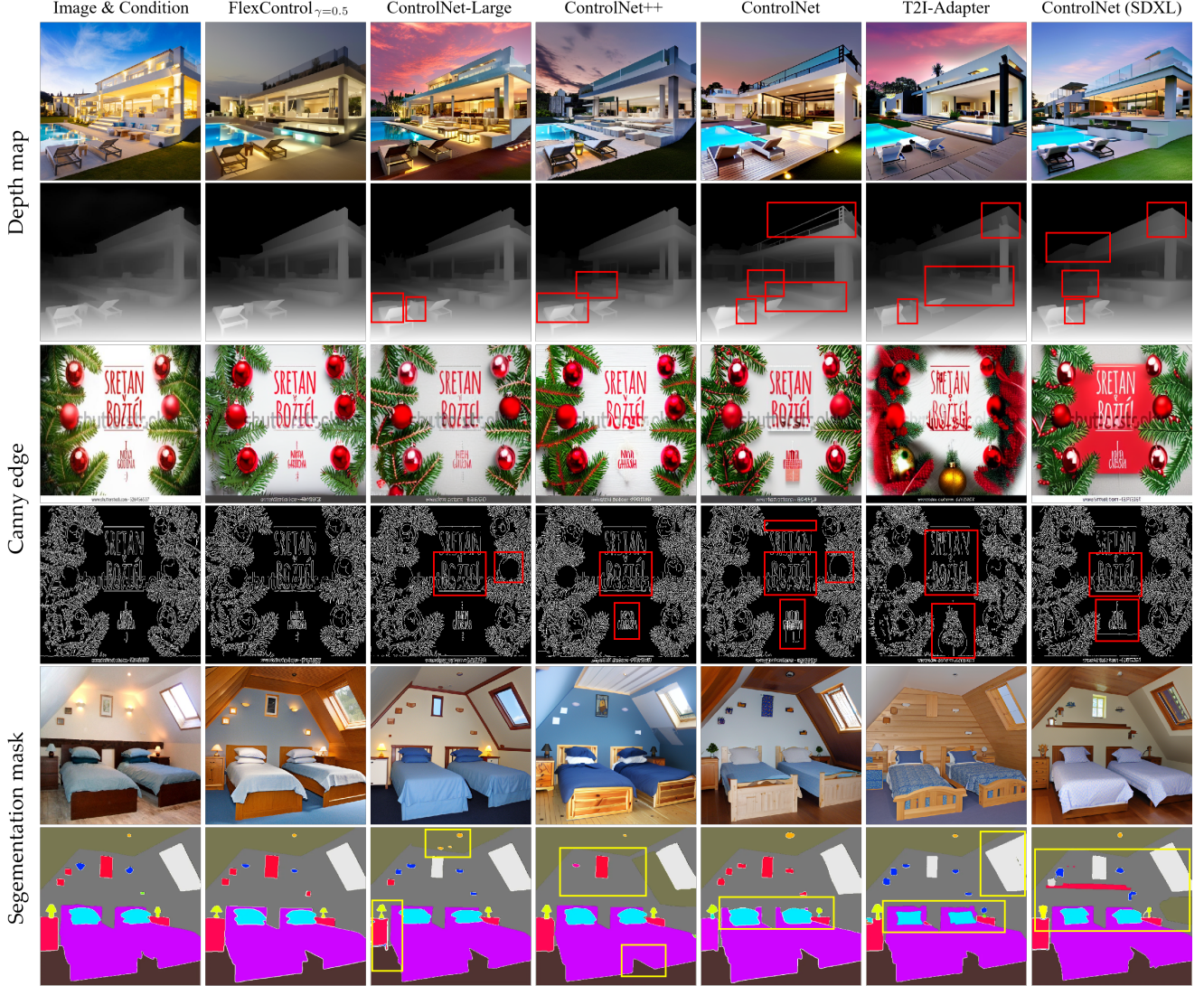


Figure 3. **Qualitative comparison of controllable generation methods.** FlexControl achieves higher fidelity and structure preservation across Depth Map, Canny Edge, and Segmentation Mask conditions, reducing distortions (boxes) seen in other methods. It better aligns with input conditions while maintaining visual quality.

4. Experiment

We evaluate FlexControl against state-of-the-art methods across different image conditions: depth maps (MultiGen-20M, [58]), canny edges (LLAVA-558K, [29]), segmentation masks (ADE20K, [59]), and *etc.*

4.1. Quantitative comparison

Comparison of image quality. To evaluate the impact of dynamic controllable generation on image quality, we compare the FID metrics of different methods across multiple conditional generation tasks (Tab. 1). We set γ to 0.5, aligning FlexControl’s FLOPs with ControlNet’s. Our model achieves superior FID results across all con-

ditions, outperforming existing methods. We also examine ControlNet-Large, which replicates the SD model as an additional network. Although its larger parameter count enhances conditional feature extraction and control, its performance remains inferior to FlexControl $_{\gamma=0.5}$. This confirms that adaptive control—selectively applying conditions instead of enforcing them across all blocks and timesteps—maximizes controllability. Beyond spatial conditions, we assess text influence using CLIP score. As shown in Tab. 1, FlexControl $_{\gamma=0.5}$ outperforms other methods, demonstrating that precise control enhances spatially guided generation without compromising text-guided synthesis. Additionally, we evaluate ControlNet and T2I-

Method	Base Model	Depth Map		Canny Edge		Seg. Mask		#Average	
		FID ↓	CLIP_score ↑	FID ↓	CLIP_score ↑	FID ↓	CLIP_score ↑	FID ↓	CLIP_score ↑
ControlNet [56]	SDXL	19.90	0.3224	22.07	0.2657	26.95	0.2495	22.97	0.2792
T2I-Adapter [32]	SDXL	19.74	0.3197	22.91	0.2614	27.54	0.2501	23.40	0.2771
GLIGEN [27]	SD1.4	18.36	0.3175	19.01	0.2520	23.79	0.2490	20.39	0.2728
T2I-Adapter [32]	SD1.5	22.52	0.3146	16.74	0.2598	24.65	0.2494	21.30	0.2728
ControlNet [56]	SD1.5	17.76	0.3245	15.23	0.2613	21.33	0.2531	18.11	0.2796
ControlNet++ [26]	SD1.5	16.66	0.3209	17.23	0.2598	19.89	0.2640	17.93	0.2816
ControlNet-Large	SD1.5	12.45	0.3492	12.92	0.2789	16.78	0.2796	14.05	0.3026
FlexControl _{$\gamma=0.5$}	SD1.5	11.65	0.3498	11.37	0.2778	14.80	0.2842	12.61	0.3039

Table 1. **Quantitative comparison of FlexControl with state-of-the-art methods.** We report FID (↓) and CLIP score (↑) on different conditioning types: Depth Map, Canny Edge, and Segmentation Mask. Lower FID indicates better image quality, while higher CLIP score reflects better alignment with textual prompts. The best results are highlighted in **red**, while the second-best results are shown in **blue**. FlexControl achieves the best overall performance, demonstrating superior fidelity and semantic alignment.

Method	Base Model	Depth Map (RMSE ↓)	Canny Edge (SSIM ↑)	Seg. Mask (mIoU ↑)
ControlNet	SDXL	0.4001	0.4178	0.2058
T2I-Adapter	SDXL	0.3976	0.3969	0.1912
GLIGEN	SD1.4	0.3882	0.4226	0.2076
T2I-Adapter	SD1.5	0.4840	0.4622	0.1839
ControlNet	SD1.5	0.2988	0.5197	0.2764
ControlNet++	SD1.5	0.2832	0.5436	0.3435
ControlNet-Large	SD1.5	0.2372	0.5642	0.3668
FlexControl _{$\gamma=0.5$}	SD1.5	0.2358	0.5612	0.3751

Table 2. **Controllability comparison across different conditioning types.** We report RMSE (↓) for Depth Map and SSIM (↑) for Canny Edge and mIoU (↑) for Seg. Mask. The best and second-best results are highlighted in **red** and **blue**. FlexControl achieve similar but slightly better controllability than ControlNet-Large with only **half**activation blocks.

Method	Base Model	Param.	FLOPs	Speed
ControlNet	SD1.5	0.36 G	233 G	5.23±0.07 it/s
ControlNet-Large	SD1.5	0.72 G	561 G	4.02±0.05 it/s
FlexControl _{$\gamma=0.7$}	SD1.5	0.73 G	393 G	4.94±0.07 it/s
FlexControl _{$\gamma=0.5$}	SD1.5	0.73 G	280 G	5.21±0.12 it/s
FlexControl _{$\gamma=0.3$}	SD1.5	0.73 G	168 G	5.64±0.12 it/s
ControlNet	SD3.0	1.06 G	3.25 T	48.34±1.78 s/it
ControlNet-Large	SD3.0	2.02 G	6.22 T	59.46±1.82 s/it
FlexControl _{$\gamma=0.7$}	SD3.0	2.03 G	4.35 T	52.15±2.86 s/it
FlexControl _{$\gamma=0.5$}	SD3.0	2.03 G	3.11 T	45.74±3.25 s/it
FlexControl _{$\gamma=0.3$}	SD3.0	2.03 G	1.86 T	40.84±3.09 s/it

Table 3. **Complexity comparison on SD1.5 and SD3.0.** We compare model parameters, FLOPs, and inference speed (it/s, iterations per second). The best values are highlighted in **red**, while the second-best values are shown in **blue**. FlexControl significant reduce overall FLOPs and inference time from ControlNet-Large.

Adapter on the SDXL backbone [36], revealing that a larger backbone does not necessarily improve image quality.

Comparison of controllability. We exam generation controllability in detail by comparing results across different spatial conditions. ControlNet and its variants generally achieve stronger controllability than other existing methods. Within a similar computational budget, FlexControl further improves controllability across various conditions. Numerically, FlexControl reduces RMSE by 6.30% and 4.74% compared to ControlNet and ControlNet++ on the depth map task. For canny edge and segmentation mask, FlexControl shows improvements of 4.15%/1.76% in SSIM and 9.87%/3.16% in mIoU, respectively. Moreover, our method outperforms ControlNet-Large on both the depth map and segmentation mask datasets, and achieves similar performance on the canny edge task. Similarly, we show the results of the SDXL-based ControlNet and T2I-Adapter show only marginal improvements for specific tasks.

4.2. Qualitative comparison

In Fig. 3, we compare different methods across depth map, canny edge, and segmentation mask tasks. All models use SD1.5 as the backbone, except for the last two columns. FlexControl consistently outperforms others in visual quality and spatial/text alignment. For depth maps, FlexControl produces smoother transitions and more natural textures. Under canny edge conditions, it better preserves edge fidelity and fine details. For segmentation masks, it enhances mask reconstruction and visual consistency. These results demonstrate FlexControl’s ability to selectively inject control information into relevant diffusion backbone blocks based on timestep and input characteristics, improving image fidelity. Finally, we compare against ControlNet and ControlNet-Large. While ControlNet-Large benefits from a larger control network for improved generation and condition alignment, FlexControl surpasses it in both accuracy and visual fidelity, showcasing the strength of our approach.

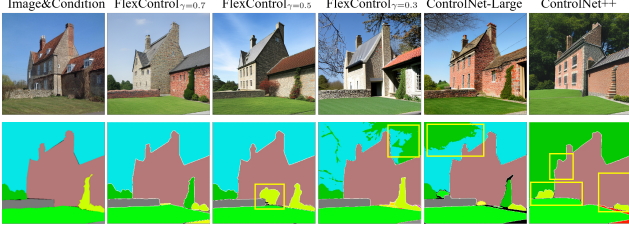


Figure 4. **Comparison of FlexControl and existing methods on SD1.5 for semantic consistency.** FlexControl achieves better semantic alignment and structure preservation with varying sparsity levels, while ControlNet-based methods show inconsistencies in segmentation accuracy (highlighted in yellow boxes). *Captions: A stone building surrounded by a stone wall and a grassy lawn.*

Method	Base Model	FID ↓	CLIP_score ↑	mIoU ↑
VQGAN [9]	✗	26.28	0.17	N/A
LDM [44]	✗	25.35	0.18	N/A
PIPT [52]	✗	19.74	0.20	N/A
ControlNet	SD1.5	21.33	0.2531	0.2764
ControlNet++	SD1.5	19.89	0.2640	0.3435
ControlNet-Large	SD1.5	16.78	0.2796	0.3668
FlexControl_{γ=0.3}	SD1.5	17.21	0.2713	0.3572
FlexControl_{γ=0.5}	SD1.5	14.80	0.2842	0.3751
FlexControl_{γ=0.7}	SD1.5	14.71	0.2840	0.3775

Table 4. **Quantitative comparison with existing methods on SD1.5.** We report FID (↓), CLIP score (↑), and mIoU (↑) across different models. The best values and second-best are highlighted in **red** and **blue**. FlexControl outperform original ControlNet with only 0.3 activation blocks, while increasing the blocks budgets observed performance increasing. Noticeable, ControlNet-Large activate all blocks yet not out-perform our methods, highlight effective of our dynamic strategy.

4.3. Ablation study

In this section, we analyze how the proportion of activated control blocks impacts FlexControl. To better understand model complexity, we present the number of parameters, FLOPs, and diffusion speed in Tab. 3. The diffusion iterations per second (*i.e.*, it/s) for SD1.5-based models and seconds per iteration (*i.e.*, s/it) for SD3.0-based models are measured on a single Nvidia RTX 2080 Ti GPU. We randomly select batch samples and compute the average single-step iteration time for each sample.

Results on UNet-based model. Recall the cost loss defined in Eq. (19), we train FlexControl with three different sparsity levels by adjusting the value of γ . For the SD1.5-based backbone, experiments are conducted on the ADE20K dataset. At $\gamma = 0.3$ (30% sparsity), FlexControl surpasses ControlNet and ControlNet++ in controllability and generation quality but falls short of ControlNet-Large. Increasing γ to 0.5 activates more control blocks, leading

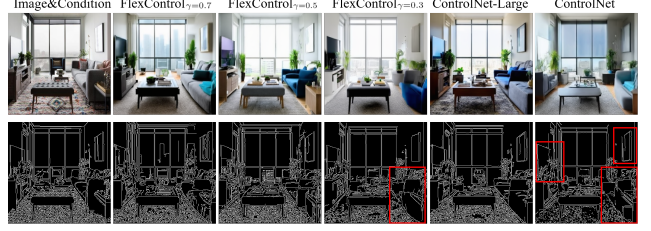


Figure 5. **Comparison of FlexControl and existing methods on SD3.0 for edge preservation.** FlexControl maintains better spatial consistency and object integrity across different sparsity levels, while ControlNet-based methods introduce distortions and inconsistencies (highlighted in red boxes). *Captions: A room with large windows, a gray sofa, a table, and a TV stand.*

Method	Base Model	FID ↓	CLIP_score ↑	SSIM ↑
ControlNet	SD3.0	27.21	0.2512	0.3749
ControlNet-Large	SD3.0	21.64	0.2690	0.4828
FlexControl_{γ=0.3}	SD3.0	24.39	0.2581	0.4286
FlexControl_{γ=0.5}	SD3.0	22.47	0.2714	0.4598
FlexControl_{γ=0.7}	SD3.0	20.54	0.2714	0.4775

Table 5. **Quantitative comparison with existing methods on SD3.0.** We report FID (↓), CLIP score (↑), and SSIM (↑). The best and second-best values are highlighted in **red** and **blue**. FlexControl outperform original ControlNet with only 0.3 activation blocks, while increasing the blocks budgets observed performance increasing even more significant improvement than we observed in SD1.5.

to performance that surpasses ControlNet-Large. Further increasing γ to 0.7 yields no significant performance gains (suggesting the dataset is already saturated by the model capacity). For visual comparisons in Fig. 4, FlexControl with $\gamma = 0.5$ and $\gamma = 0.7$ demonstrate superior structure preservation and mask information reconstruction. Meanwhile, the more lightweight configuration with $\gamma = 0.3$ achieves a generation quality comparable to ControlNet++ and ControlNet-Large.

Results on DiT-based model. For the SD3.0-based backbone, experiments were conducted on the LLAVA-558K dataset. As detailed in Tab. 5, FlexControl_{γ=0.3} and FlexControl_{γ=0.5} outperform ControlNet with fewer FLOPs. Notably, while ControlNet has half as many blocks as the backbone, each control block’s output is shared by two adjacent backbone blocks, providing more conditional controls than FlexControl at all sparsity levels. FlexControl_{γ=0.7} achieves superior image quality and comparable controllability to ControlNet-Large while being more efficient. Visualization results in Fig. 5 further demonstrate the advantage of FlexControl in edge reproduction and image fidelity over ControlNet.

5. Conclusion

We presented FlexControl, a dynamic framework that reimagines controlled diffusion by replacing heuristic block selection with a trainable, computation-aware gating mechanism. By enabling adaptive activation of control blocks during denoising, FlexControl eliminates manual architectural tuning, reduces computational overhead, and maintains or improves output fidelity across diverse tasks and architectures (UNet, DiT). Our experiments demonstrate that flexibility and efficiency need not be mutually exclusive in controllable generation—intelligent, data-driven activation strategies can outperform rigid, handcrafted designs. This work paves the way for future research into lightweight, generalizable control mechanisms for increasingly complex generative pipelines. We also conduct a further investigation on the dynamic activation route, which has been listed in Sec. A3.

References

- [1] Fan Bao, Shen Nie, Kaiwen Xue, Yue Cao, Chongxuan Li, Hang Su, and Jun Zhu. All are worth words: A vit backbone for diffusion models. In *Proceedings of the IEEE/CVF conference on computer vision and pattern recognition*, pages 22669–22679, 2023. 2
- [2] Fan Bao, Shen Nie, Kaiwen Xue, Chongxuan Li, Shi Pu, Yaole Wang, Gang Yue, Yue Cao, Hang Su, and Jun Zhu. One transformer fits all distributions in multi-modal diffusion at scale. In *International Conference on Machine Learning*, pages 1692–1717. PMLR, 2023. 2
- [3] John Canny. A computational approach to edge detection. *IEEE Transactions on pattern analysis and machine intelligence*, pages 679–698, 1986. 12
- [4] Minghao Chen, Iro Laina, and Andrea Vedaldi. Training-free layout control with cross-attention guidance. In *Proceedings of the IEEE/CVF Winter Conference on Applications of Computer Vision*, pages 5343–5353, 2024. 2
- [5] Zhe Chen, Jiannan Wu, Wenhai Wang, Weijie Su, Guo Chen, Sen Xing, Muyan Zhong, Qinglong Zhang, Xizhou Zhu, Lewei Lu, et al. Internvl: Scaling up vision foundation models and aligning for generic visual-linguistic tasks. In *Proceedings of the IEEE/CVF Conference on Computer Vision and Pattern Recognition*, pages 24185–24198, 2024. 12
- [6] Zhaoli Deng, Kaibin Zhou, Fanyi Wang, and Zhenpeng Mi. Repcontrolnet: Controlnet reparameterization. *arXiv preprint arXiv:2408.09240*, 2024. 3
- [7] Prafulla Dhariwal and Alexander Nichol. Diffusion models beat gans on image synthesis. *Advances in neural information processing systems*, 34:8780–8794, 2021. 2
- [8] Xiaohan Ding, Xiangyu Zhang, Ningning Ma, Jungong Han, Guiguang Ding, and Jian Sun. Repvgg: Making vgg-style convnets great again. In *Proceedings of the IEEE/CVF conference on computer vision and pattern recognition*, pages 13733–13742, 2021. 3
- [9] Patrick Esser, Robin Rombach, and Bjorn Ommer. Taming transformers for high-resolution image synthesis. In *Proceedings of the IEEE/CVF conference on computer vision and pattern recognition*, pages 12873–12883, 2021. 8
- [10] Patrick Esser, Sumith Kulal, Andreas Blattmann, Rahim Entezari, Jonas Müller, Harry Saini, Yam Levi, Dominik Lorenz, Axel Sauer, Frederic Boesel, et al. Scaling rectified flow transformers for high-resolution image synthesis, march 2024. URL <http://arxiv.org/abs/2403.03206>, 2024. 3, 12, 13
- [11] Patrick Esser, Sumith Kulal, Andreas Blattmann, Rahim Entezari, Jonas Müller, Harry Saini, Yam Levi, Dominik Lorenz, Axel Sauer, Frederic Boesel, et al. Scaling rectified flow transformers for high-resolution image synthesis. In *Forty-first International Conference on Machine Learning*, 2024. 2
- [12] Gongfan Fang, Xinyin Ma, and Xinchao Wang. Structural pruning for diffusion models. *Advances in Neural Information Processing Systems*, 2023. 3
- [13] Alireza Ganjdanesh, Reza Shirkavand, Shangkian Gao, and Heng Huang. Not all prompts are made equal: Prompt-based pruning of text-to-image diffusion models. *arXiv preprint arXiv:2406.12042*, 2024. 3
- [14] Martin Heusel, Hubert Ramsauer, Thomas Unterthiner, Bernhard Nessler, and Sepp Hochreiter. Gans trained by a two time-scale update rule converge to a local nash equilibrium. *Advances in neural information processing systems*, 30, 2017. 13
- [15] Jonathan Ho, Ajay Jain, and Pieter Abbeel. Denoising diffusion probabilistic models. *Advances in neural information processing systems*, 33:6840–6851, 2020. 3
- [16] Yi-Ting Hsiao, Siavash Khodadadeh, Kevin Duarte, Wei-An Lin, Hui Qu, Mingi Kwon, and Ratheesh Kalarot. Plug-and-play diffusion distillation. In *Proceedings of the IEEE/CVF Conference on Computer Vision and Pattern Recognition*, pages 13743–13752, 2024. 3
- [17] Minghui Hu, Jianbin Zheng, Daqing Liu, Chuanxia Zheng, Chaoyue Wang, Dacheng Tao, and Tat-Jen Cham. Cocktail: Mixing multi-modality control for text-conditional image generation. In *Thirty-seventh Conference on Neural Information Processing Systems*, 2023. 2
- [18] Lianghua Huang, Di Chen, Yu Liu, Yujun Shen, Deli Zhao, and Jingren Zhou. Composer: Creative and controllable image synthesis with composable conditions. *arXiv preprint arXiv:2302.09778*, 2023. 2
- [19] Ziqi Huang, Tianxing Wu, Yuming Jiang, Kelvin CK Chan, and Ziwei Liu. Reversion: Diffusion-based relation inversion from images. *arXiv preprint arXiv:2303.13495*, 2023.
- [20] Ruixiang Jiang, Can Wang, Jingbo Zhang, Menglei Chai, Mingming He, Dongdong Chen, and Jing Liao. Avatarcraft: Transforming text into neural human avatars with parameterized shape and pose control. In *Proceedings of the IEEE/CVF International Conference on Computer Vision*, pages 14371–14382, 2023. 2
- [21] Xuan Ju, Ailing Zeng, Chenchen Zhao, Jianan Wang, Lei Zhang, and Qiang Xu. Humansd: A native skeleton-guided diffusion model for human image generation. In *Proceedings of the IEEE/CVF International Conference on Computer Vision*, pages 15988–15998, 2023. 2

- [22] Xuan Ju, Xian Liu, Xintao Wang, Yuxuan Bian, Ying Shan, and Qiang Xu. Brushnet: A plug-and-play image inpainting model with decomposed dual-branch diffusion. *arXiv preprint arXiv:2403.06976*, 2024. **2, 4**
- [23] Bo-Kyeong Kim, Hyoung-Kyu Song, Thibault Castells, and Shinkook Choi. On architectural compression of text-to-image diffusion models. *arXiv preprint arXiv:2305.15798*, 2023. **3**
- [24] Diederik Kingma, Tim Salimans, Ben Poole, and Jonathan Ho. Variational diffusion models. *Advances in neural information processing systems*, 34:21696–21707, 2021. **2**
- [25] Yunsung Lee, JinYoung Kim, Hyojun Go, Myeongho Jeong, Shinhyeok Oh, and Seungtaek Choi. Multi-architecture multi-expert diffusion models. In *Proceedings of the AAAI Conference on Artificial Intelligence*, pages 13427–13436, 2024. **3**
- [26] Ming Li, Taojiannan Yang, Huafeng Kuang, Jie Wu, Zhaoning Wang, Xuefeng Xiao, and Chen Chen. Controlnet++: Improving conditional controls with efficient consistency feedback. In *European Conference on Computer Vision*, pages 129–147. Springer, 2025. **2, 7**
- [27] Yuheng Li, Haotian Liu, Qingyang Wu, Fangzhou Mu, Jianwei Yang, Jianfeng Gao, Chunyuan Li, and Yong Jae Lee. Gligen: Open-set grounded text-to-image generation. In *Proceedings of the IEEE/CVF Conference on Computer Vision and Pattern Recognition*, pages 22511–22521, 2023. **2, 7**
- [28] Yaron Lipman, Ricky TQ Chen, Heli Ben-Hamu, Maximilian Nickel, and Matt Le. Flow matching for generative modeling. In *International Conference on Learning Representations*, 2023. **3**
- [29] Haotian Liu, Chunyuan Li, Qingyang Wu, and Yong Jae Lee. Visual instruction tuning. *Advances in neural information processing systems*, 36, 2024. **6, 12**
- [30] Xingchao Liu, Chengyue Gong, and Qiang Liu. Flow straight and fast: Learning to generate and transfer data with rectified flow. *arXiv preprint arXiv:2209.03003*, 2022. **3**
- [31] Xingchao Liu, Xiwen Zhang, Jianzhu Ma, Jian Peng, et al. Instaflo: One step is enough for high-quality diffusion-based text-to-image generation. In *The Twelfth International Conference on Learning Representations*, 2023. **3**
- [32] Chong Mou, Xintao Wang, Liangbin Xie, Yanze Wu, Jian Zhang, Zhongang Qi, and Ying Shan. T2i-adapter: Learning adapters to dig out more controllable ability for text-to-image diffusion models. In *Proceedings of the AAAI Conference on Artificial Intelligence*, pages 4296–4304, 2024. **1, 2, 7**
- [33] Alex Nichol, Prafulla Dhariwal, Aditya Ramesh, Pranav Shyam, Pamela Mishkin, Bob McGrew, Ilya Sutskever, and Mark Chen. Glide: Towards photorealistic image generation and editing with text-guided diffusion models. In *International conference on machine learning*, 2022. **2**
- [34] William Peebles and Saining Xie. Scalable diffusion models with transformers. In *Proceedings of the IEEE/CVF International Conference on Computer Vision*, pages 4195–4205, 2023. **2**
- [35] Bohao Peng, Jian Wang, Yuechen Zhang, Wenbo Li, Ming-Chang Yang, and Jiaya Jia. Controlnext: Powerful and efficient control for image and video generation. *arXiv preprint arXiv:2408.06070*, 2024. **3**
- [36] Dustin Podell, Zion English, Kyle Lacey, Andreas Blattmann, Tim Dockhorn, Jonas Müller, Joe Penna, and Robin Rombach. Sdxl: Improving latent diffusion models for high-resolution image synthesis. *arXiv preprint arXiv:2307.01952*, 2023. **2, 7**
- [37] Can Qin, Shu Zhang, Ning Yu, Yihao Feng, Xinyi Yang, Yingbo Zhou, Huan Wang, Juan Carlos Niebles, Caiming Xiong, Silvio Savarese, et al. Unicontrol: A unified diffusion model for controllable visual generation in the wild. *arXiv preprint arXiv:2305.11147*, 2023. **2**
- [38] Alec Radford, Jong Wook Kim, Chris Hallacy, Aditya Ramesh, Gabriel Goh, Sandhini Agarwal, Girish Sastry, Amanda Askell, Pamela Mishkin, Jack Clark, et al. Learning transferable visual models from natural language supervision. In *International conference on machine learning*, pages 8748–8763. PMLR, 2021. **2, 13**
- [39] Colin Raffel, Noam Shazeer, Adam Roberts, Katherine Lee, Sharan Narang, Michael Matena, Yanqi Zhou, Wei Li, and Peter J Liu. Exploring the limits of transfer learning with a unified text-to-text transformer. *Journal of machine learning research*, 21(140):1–67, 2020. **2**
- [40] Samyam Rajbhandari, Jeff Rasley, Olatunji Ruwase, and Yuxiong He. Zero: Memory optimizations toward training trillion parameter models. In *SC20: International Conference for High Performance Computing, Networking, Storage and Analysis*, pages 1–16. IEEE, 2020. **13**
- [41] Yongming Rao, Wenliang Zhao, Benlin Liu, Jiwen Lu, Jie Zhou, and Cho-Jui Hsieh. Dynamicvit: Efficient vision transformers with dynamic token sparsification. *Advances in neural information processing systems*, 34:13937–13949, 2021. **5**
- [42] Yongming Rao, Zuyan Liu, Wenliang Zhao, Jie Zhou, and Jiwen Lu. Dynamic spatial sparsification for efficient vision transformers and convolutional neural networks. *IEEE Transactions on Pattern Analysis and Machine Intelligence*, 45(9):10883–10897, 2023. **5**
- [43] Mengwei Ren, Mauricio Delbracio, Hossein Talebi, Guido Gerig, and Peyman Milanfar. Image deblurring with domain generalizable diffusion models. *arXiv preprint arXiv:2212.01789*, 1, 2022. **2**
- [44] Robin Rombach, Andreas Blattmann, Dominik Lorenz, Patrick Esser, and Björn Ommer. High-resolution image synthesis with latent diffusion models. In *Proceedings of the IEEE/CVF conference on computer vision and pattern recognition*, pages 10684–10695, 2022. **2, 8**
- [45] Olaf Ronneberger, Philipp Fischer, and Thomas Brox. U-net: Convolutional networks for biomedical image segmentation. In *Medical image computing and computer-assisted intervention—MICCAI 2015: 18th international conference, Munich, Germany, October 5–9, 2015, proceedings, part III 18*, pages 234–241. Springer, 2015. **2**
- [46] Chitwan Saharia, William Chan, Saurabh Saxena, Lala Li, Jay Whang, Emily L Denton, Kamyar Ghasemipour, Raphael Gontijo Lopes, Burcu Karagol Ayan, Tim Salimans, et al. Photorealistic text-to-image diffusion models with deep language understanding. *Advances in neural information processing systems*, 35:36479–36494, 2022. **2**

- [47] Christoph Schuhmann, Romain Beaumont, Richard Vencu, Cade Gordon, Ross Wightman, Mehdi Cherti, Theo Coombes, Aarush Katta, Clayton Mullis, Mitchell Wortsman, et al. Laion-5b: An open large-scale dataset for training next generation image-text models. *Advances in Neural Information Processing Systems*, 35:25278–25294, 2022. 12
- [48] Jascha Sohl-Dickstein, Eric Weiss, Niru Maheswaranathan, and Surya Ganguli. Deep unsupervised learning using nonequilibrium thermodynamics. In *International conference on machine learning*, pages 2256–2265. PMLR, 2015. 2
- [49] Jiaming Song, Chenlin Meng, and Stefano Ermon. Denoising diffusion implicit models. In *International Conference on Learning Representations*, 2021. 13
- [50] Stability. Stable diffusion v1.5 model card. <https://huggingface.co/runwayml/stable-diffusion-v1-5>, 2022. 1, 2, 12
- [51] Zhengzhong Tu, Hossein Talebi, Han Zhang, Feng Yang, Peyman Milanfar, Alan Bovik, and Yinxiao Li. Maxvit: Multi-axis vision transformer. In *European conference on computer vision*, pages 459–479. Springer, 2022. 2
- [52] Tengfei Wang, Ting Zhang, Bo Zhang, Hao Ouyang, Dong Chen, Qifeng Chen, and Fang Wen. Pretraining is all you need for image-to-image translation. *arXiv preprint arXiv:2205.12952*, 2022. 8
- [53] Xudong Wang, Trevor Darrell, Sai Saketh Rambhatla, Rohit Girdhar, and Ishan Misra. Instancediffusion: Instance-level control for image generation. In *Proceedings of the IEEE/CVF Conference on Computer Vision and Pattern Recognition*, pages 6232–6242, 2024. 2
- [54] Zhengyuan Yang, Jianfeng Wang, Zhe Gan, Linjie Li, Kevin Lin, Chenfei Wu, Nan Duan, Zicheng Liu, Ce Liu, Michael Zeng, et al. Reco: Region-controlled text-to-image generation. In *Proceedings of the IEEE/CVF Conference on Computer Vision and Pattern Recognition*, pages 14246–14255, 2023. 2
- [55] Huijie Zhang, Yifu Lu, Ismail Alkhouri, Saiprasad Ravishankar, Dogyoon Song, and Qing Qu. Improving efficiency of diffusion models via multi-stage framework and tailored multi-decoder architectures. *arXiv preprint arXiv:2312.09181*, 2023. 3
- [56] Lvmin Zhang, Anyi Rao, and Maneesh Agrawala. Adding conditional control to text-to-image diffusion models. In *Proceedings of the IEEE/CVF International Conference on Computer Vision*, pages 3836–3847, 2023. 1, 2, 4, 7, 13
- [57] Tianjun Zhang, Yi Zhang, Vibhav Vineet, Neel Joshi, and Xin Wang. Controllable text-to-image generation with gpt-4. *arXiv preprint arXiv:2305.18583*, 2023. 2
- [58] Shihao Zhao, Dongdong Chen, Yen-Chun Chen, Jianmin Bao, Shaozhe Hao, Lu Yuan, and Kwan-Yee K Wong. Uni-controlnet: All-in-one control to text-to-image diffusion models. *Advances in Neural Information Processing Systems*, 36, 2024. 2, 6, 12
- [59] Bolei Zhou, Hang Zhao, Xavier Puig, Sanja Fidler, Adela Barriuso, and Antonio Torralba. Scene parsing through ade20k dataset. In *Proceedings of the IEEE conference on computer vision and pattern recognition*, pages 633–641, 2017. 6, 12
- [60] Dewei Zhou, You Li, Fan Ma, Xiaoting Zhang, and Yi Yang. Mige: Multi-instance generation controller for text-to-image synthesis. In *Proceedings of the IEEE/CVF Conference on Computer Vision and Pattern Recognition*, pages 6818–6828, 2024. 2

FlexControl: Computation-Aware ControlNet with Differentiable Router for Text-to-Image Generation

Supplementary Material

The supplementary material presents the following sections to strengthen the main manuscript:

- Pseudocode of our algorithm.
- Implementation details.
- Dynamic route exploration.
- More visualization

A1. Pseudocode of Our Algorithm

Algorithm 1 Inference procedure

Input: conditional image \mathbf{c}_s , text prompt \mathbf{c}_t , timestep T .
Fully-trained FlexControl, pre-trained SD model.

```

1: for each  $i \in [T, 1]$  do
2:   for each  $l \in \text{Blocks}$  do
3:     /* The value of  $\mathcal{M}_l$  is adjusted with input  $\mathbf{h}_{l-1}$  */
4:     Compute  $\mathcal{M}_l$  though router unit
5:     if  $\mathcal{M}_l = 1$  then
6:       /* Extract latent features from conditions */
7:       Compute  $\mathbf{h}_l$  though Eq. (8)
8:       /* Feature transformation by zero modules */
9:       Transform  $\mathbf{h}_l$  to  $\mathbf{y}_c^l$  though Eq. (9)
10:      /* Inject modal information into feature space */
11:      Inject  $\mathbf{y}_c^l$  to SD model though Eq. (7)
12:    else
13:      /* Align the dimension of feature mapping */
14:      Bypass  $\mathcal{F}_l$  and  $\mathcal{Z}_l$  though  $\text{skip}_l(\cdot)$ 
15:    end if
16:  end for
17:  /* DDIM sampler for SD1.5-based models */
18:  /* RFlow sampler for SD3.0-based models */
19:  Predict denoised image with  $T$ -step sampling
20: end for
21: return  $\mathbf{x}_0$ 

```

A2. Implementation Details

We implement FlexControl based on SD1.5 [50] and SD3.0 [10]. The experiments are carried out under various conditions, mainly including depth map, canny edge and segmentation mask. The following is a description of the experimental details.

Training dataset. The experiment involves three types of conditional maps:

- *Depth map.* In this application, we use MultiGen-20M proposed by [58] as training data, which is a subset

Algorithm 2 Training procedure

Input: Dataset $\mathcal{D}(x, \mathbf{c}_s, \mathbf{c}_t)$, hyperparameters $(\tau, \gamma, \lambda_C)$.
Initialized FlexControl model, pre-trained SD model.

```

1: Turn off the router units for warm-up training
2: Turn on the router units for end-to-end training
3: while not converged do
4:   Sample timestep  $t \sim \text{Uniform}(0, 1)$ 
5:   Sample noise  $\epsilon \sim \mathcal{N}(\mathbf{0}, \mathbf{I})$ 
6:   /* Eq. (2) is used for SD1.5-based models */
7:   /* Eq. (5) is used for SD3.0-based models */
8:   Transfer image  $\mathbf{x}_0$  to noisy image  $\mathbf{x}_t$ 
9:   /* Based on Eqs. (7), (16) and (17) */
10:   $\mathbf{y}_{pred}, \mathcal{M} = \hat{\epsilon}_\theta(\mathbf{x}_t, \mathbf{c}_t, \mathbf{c}_s, t)$ 
11:  /*  $\mathcal{L}_{SD}$  is used to optimize generation effect */
12:  Compute MSE loss  $\mathcal{L}_{SD}$  though Eq. (18)
13:  /*  $\mathcal{L}_C$  is used to control sparsity */
14:  Compute cost loss  $\mathcal{L}_C$  though Eq. (19)
15:  /*  $\mathcal{L}_\theta$  is used as final optimization goal */
16:  Compute final loss  $\mathcal{L}_\theta$  though Eq. (20)
17:  /* Freeze the weight parameters of the backbone */
18:   $\theta = \theta - lr \nabla_\theta \mathcal{L}_\theta(\mathbf{x}_t, \mathbf{y}_{pred}, \mathcal{M})$ 
19: end while
20: return fully-trained FlexControl

```

of LAION-Aesthetics [47] and contains over 2 million depth-image-caption pairs, and 5K test samples.

- *Canny edge.* For the condition of the canny edge, we use the LLaVA-558K [29] dataset to verify the model, which contains 558K image-caption pairs. A canny edge detector [3] is used to convert RGB images to edge images, and the low and high threshold of hysteresis procedure in this process are set to 100 and 200, respectively.
- *Segmentation mask.* For the segmentation mask, we use the ADE20K [59] dataset for model training. This dataset contains a total of 27K segmentation image pairs, 25K for training and 2K for testing. InternVL2-2B [5] is used to generate captions for RGB images with instruction “Please use a brief sentence with as few words as possible to summarize the picture”.

Training settings. During the training procedure, we uniformly use the AdamW optimizer with a learning rate of 1×10^{-5} . For SD1.5-based models, half-precision floating-point (Float16) is used for mixed precision training, original images and conditional images are resized to 512×512 , and batchsize and gradient accumulation steps are set to 4

and 32, respectively. When turning to SD3.0, we further use DeepSpeed [40] Zero-2 to accelerate the training process, the resolution of 1024×1024 is used, and the batch-size and gradient accumulation steps are set to 4 and 8. We set the maximum training iterations to 50k and 25k for the models based on SD1.5 and SD3.0, respectively. For the threshold parameter τ required by the Gumbel-Sigmoid activation function in the router unit, we set it to 0.5, and the hyperparameter λ_C in the loss function \mathcal{L}_θ is set to 0.5, the value of γ depends on the target sparsity. When training UNet-based ControlNet-large and FlexControl, we remove the residual connection between the encoder blocks and the decoder blocks of the control network. For the problem of the weight dimension cannot be aligned when initializing the decoder blocks of the control network using SD1.5’s pre-trained weights caused by this operation, we solve it by reinitializing these weights. The models based on SD1.5 and SD3.0 are trained with 2 and 8 Nvidia-A100 (40G) GPUs, respectively.

Our FlexControl follows the core design philosophy of [56], the trainable blocks are initialized with the pre-trained weight parameters of the SD model, and zero modules are added at the same time, which leads to the conditional mappings generated at the early training stage do not have the ability to control generation effectively. Therefore, we first fix mask \mathcal{M} to 1 for warm-up training in the early training stage, *e.g.*, 10K steps for SD1.5-based FlexControl and 5K steps for SD3-based FlexControl in our implementation, and then turn on the router unit to train together with the copy blocks. This helps the whole training procedure move in the right direction.

Benchmark and metrics. For quantitative comparison, we present the Frechet Inception Distance (FID) [14] and CLIP_score [38] to assess the quality of the generated images. In addition, we calculate RMSE, SSIM and mIoU on depth map, canny edge and segmentation mask respectively, to evaluate the controllability of image generation. Finally, we emphatically compare the computational complexity. The results of depth map are tested on MultiGen-20M test set and the results of canny edge and segmentation mask are tested on COCO validation set, which contains 5,000 samples and each sample contains five text descriptions, we randomly choose one text of each sample as input during testing. For sampling, we employ DDIM [49] and RFlow [10] sampler, implementing 20 denoising steps to generate images without incorporating any negative prompts. We generate five groups of images, and the average results are reported.

A3. Dynamic Route Exploration

In order to improve the parameter utilization of ControlNet in the application, we explore how the router unit activates

the control block to generate conditional controls.

It can be seen from Fig. 1(c), both SD1.5 based on UNet and SD3.0 based on DiT, the activation of control blocks presents a sparse distribution in the early denoising stage and a dense distribution in the late stage. This means that the late denoising stage plays a more important role in controllable image generation. Since the early sampling is mainly responsible for generating the global structure and low-frequency information of the image (*e.g.*, the approximate shape of the object, the distribution of the components), while the late sampling is mainly responsible for generating high-frequency information and correcting complex details (*e.g.*, edge, texture). For this, more conditional control signals are necessary. Moreover, the generation deviation in the early stage is relatively small and can be rectified by subsequent sampling. If the sampling error in the later stage is large, the conditional consistency will be destroyed, resulting in loss of control effect.

Based on the above findings, we can conclude that using unified control scheme in any case is an inefficient control mode, which leads to most of the conditional controls added in the early stage not playing the ideal role, and there will be insufficient conditional controls added in the late stage. Therefore, our dynamic control method can further release the performance of the controllable generation model by solving this problem. Next, we do a more detailed analysis of the different settings.

First, we test the activation time and position of the control block under different number of timestep settings with γ set to 0.5 (*i.e.*, approximately 50% sparsity). We set the timesteps to 10, 20 and 50 respectively. As shown in Fig. A1, it can be found that the pattern under different settings is basically the same as above. In the early stage, only a few blocks are activated, mainly concentrated in the head and tail. As the number of sampling steps increases, more blocks are activated. Until the middle stage of sampling, most of the blocks are activated.

Next, we test the activation of control blocks under different sparsity. We approximate 30%, 50%, and 70% sparsity by setting γ to 0.3, 0.5, and 0.7. It can be seen from Fig. A2, when 30% sparsity is used, fewer blocks are activated at the late stage, and even some control blocks are not activated at all. When the sparsity increased to 70%, more middle blocks are activated in the early sampling period, and almost all blocks are activated in the late sampling period.

In addition, we discuss the activation of various spatial conditions at each timestep. As shown in Fig. A3, similar trend is found across different types of conditional maps, which proves the generalization of the above findings. In addition, there are some differences in activation details, which means that the router unit makes independent judgments on different conditional samples and plans specific

activation routes for them. Due to the differences in feature distribution and information in the samples, this fine-grained control is particularly important for striking a balance between performance and efficiency.

Relying on the above findings, when we apply ControlNet or similar architectures in practice, only activating the head and tail blocks in the early stage, or even activating ControlNet only in the late stage, can simply improve the inference efficiency, and no retraining is involved.

A4. More Visualization



Figure A1. **The distribution of activated control blocks under different timesteps.** The hyperparameter γ is set to 0.5 to approximate 50% sparsity, and timestep is set to 10, 20 and 50 respectively. The first line shows the results of the model based on SD1.5, and the second line shows the results of the model based on SD3.0. ■ and ■ denotes activated and inactivated blocks, respectively.

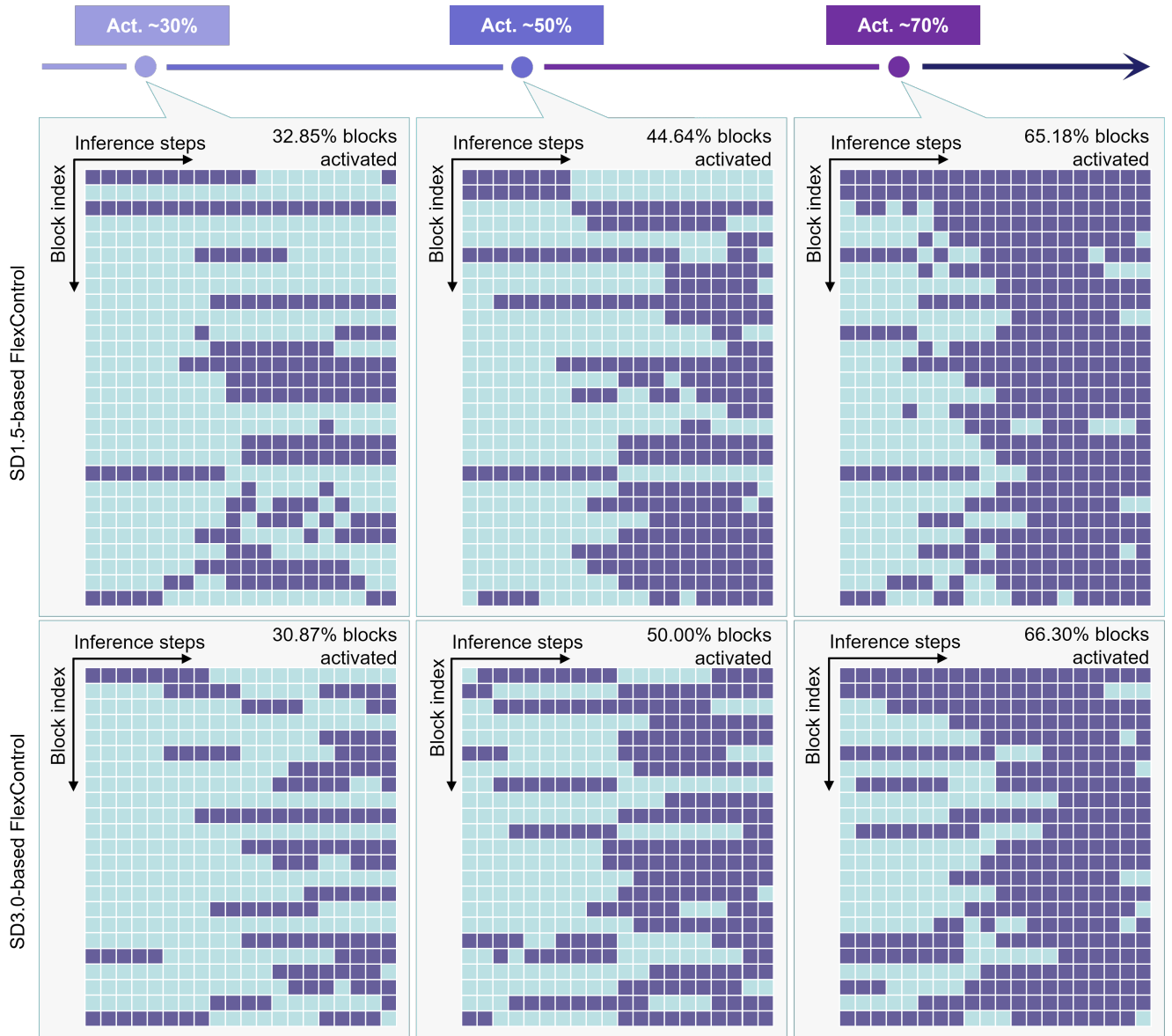


Figure A2. **The distribution of activated control blocks under different sparsity.** The hyperparameter γ is set to 0.3, 0.5 and 0.7 to approximate 30%, 50%, and 70% sparsity, and the timestep is set to 20. The first line shows the results of the model based on SD1.5, and the second line shows the results of the model based on SD3.0.

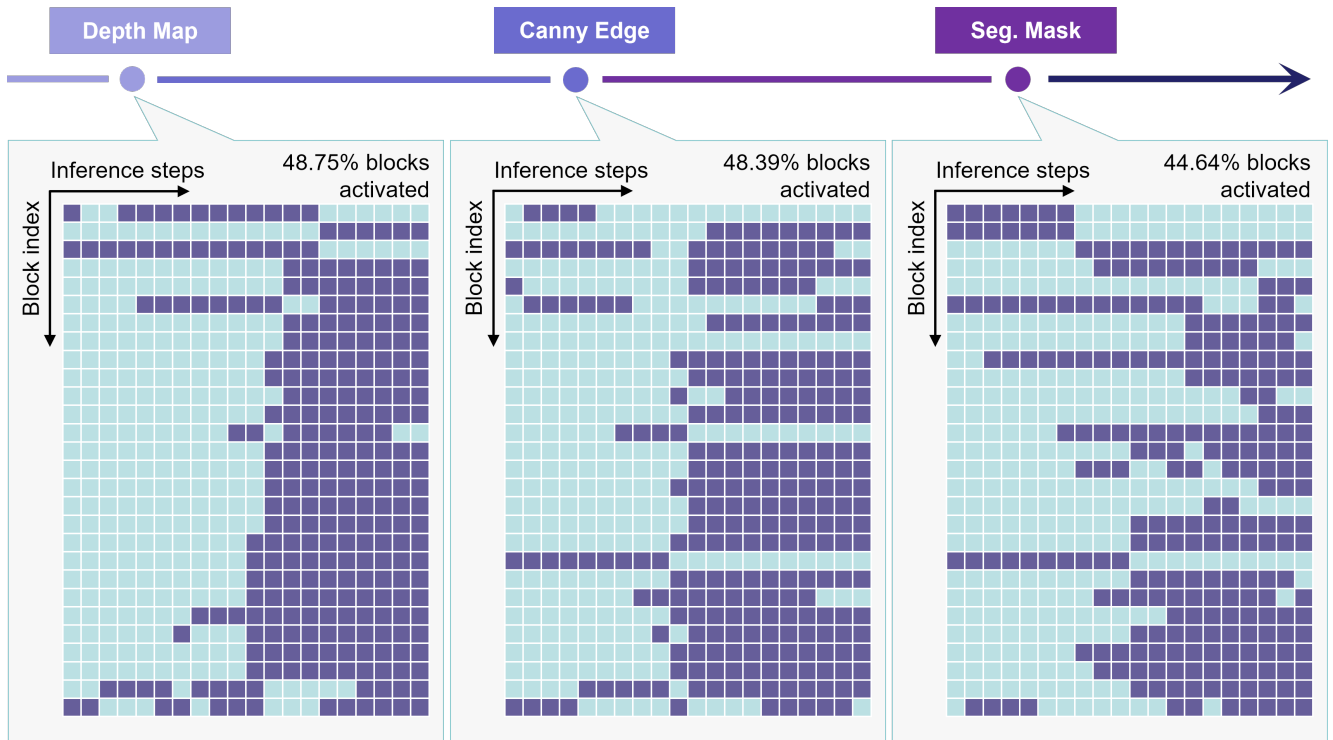


Figure A3. **The distribution of activated control blocks under various conditional controls.** The hyperparameter γ is set to 0.5 to approximate 50% sparsity, and the timestep is set to 20.

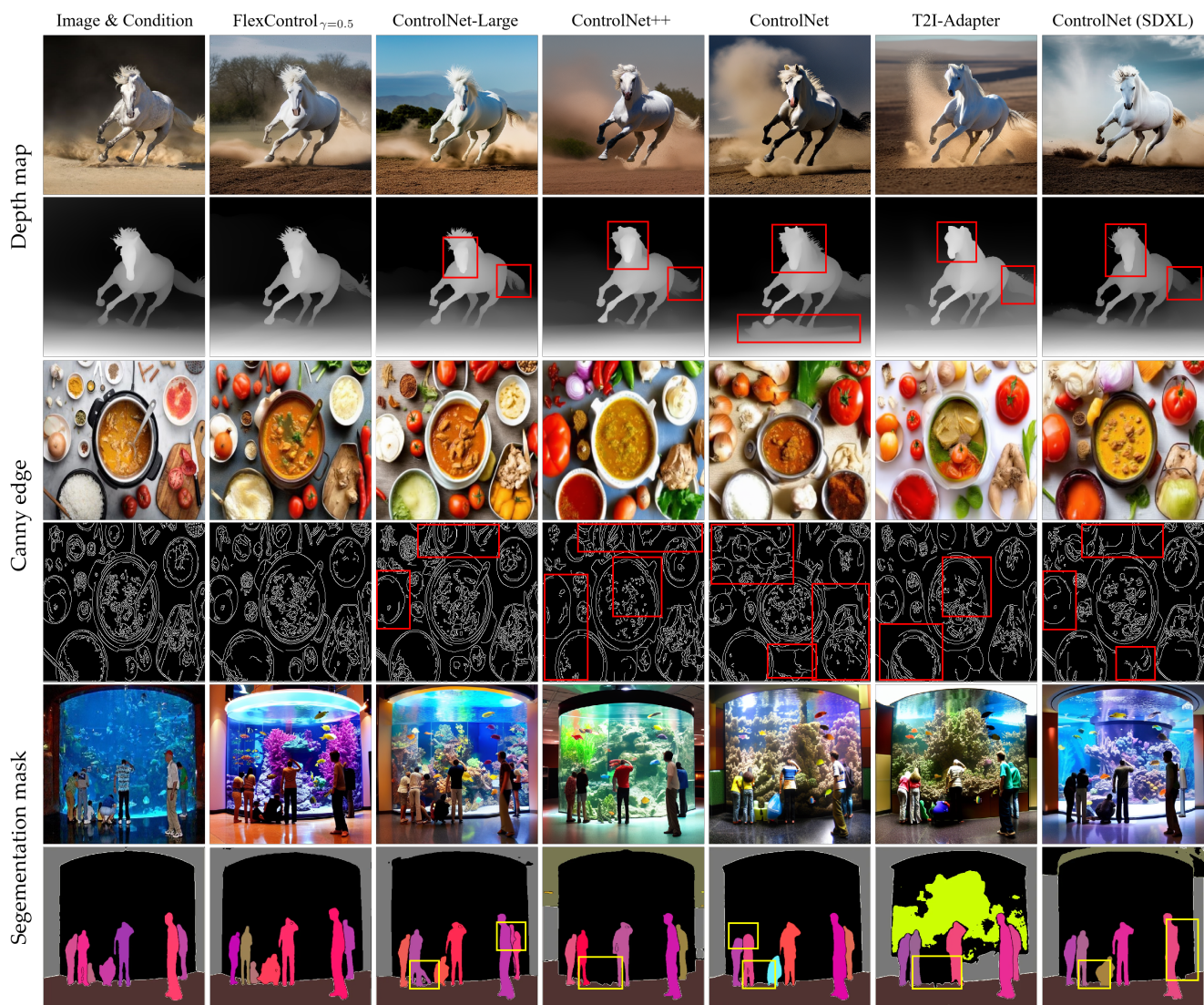


Figure A4. **Visualization comparison** with state-of-the-art controllable generation methods on various conditions. Except for the last two columns, the other models use SD1.5 as the backbone. *Captions: A white stallion horse galloping furiously kicking up the dust behind it. Ingredients of curry, including onions, garlic, chili, and tomatoes. A group of people are observing an aquarium filled with colorful fish.*

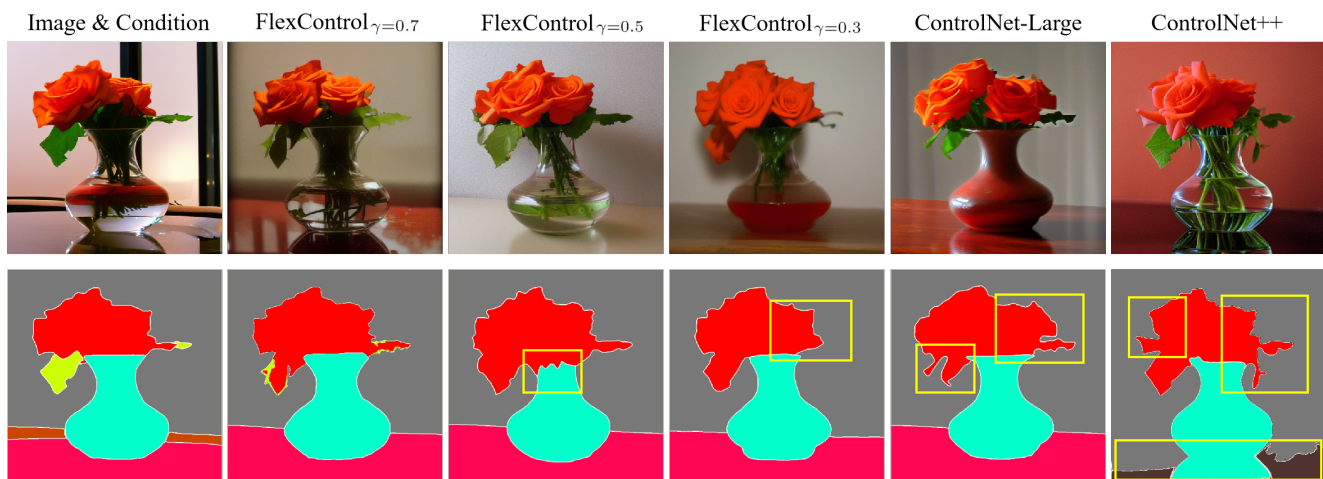


Figure A5. **Visualization comparison** of FlexControl and existing methods on SD1.5 for semantic consistency. *Captions: A reddish rose in a vase filled with water on the table.*

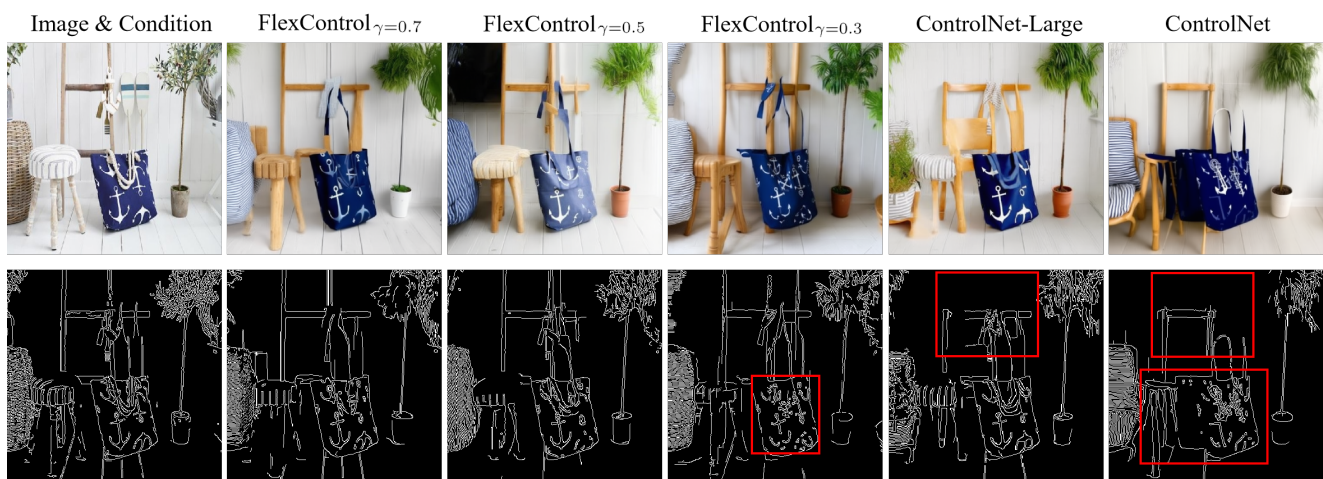


Figure A6. **Visualization comparison** of FlexControl and existing methods on SD3.0 for edge preservation. *Captions: A wooden chair with a striped cushion, a navy blue tote bag with anchors, and a potted plant are arranged on a white floor against a white wooden wall.*